Atmos. Meas. Tech. Discuss., 7, 12283–12322, 2014
www.atmos-meas-tech-discuss.net/7/12283/2014/
doi:10.5194/amtd-7-12283-2014

Atmospheric Measurement Techniques Discussions
Open Access

ALADINA – an unmanned research aircraft for observing vertical and horizontal distributions of ultrafine particles within the atmospheric boundary layer

B. Altstädter[1], A. Platis[2], B. Wehner[3], A. Scholtz[4], A. Lampert[1], N. Wildmann[2], M. Hermann[3], R. Käthner[3], J. Bange[2], and H. Baars[3]

[1]Institute of Flight Guidance, Technische Universität Braunschweig, Braunschweig, Germany
[2]Center for Applied Geosciences, Eberhard Karls Universität Tübingen, Tübingen, Germany
[3]Leibniz Institute for Tropospheric Research, Leipzig, Germany
[4]Institute of Aerospace Systems, Technische Universität Braunschweig, Braunschweig, Germany

Received: 1 September 2014 – Accepted: 18 November 2014 – Published: 10 December 2014

Correspondence to: B. Altstädter (b.altstaedter@tu-braunschweig.de)

Published by Copernicus Publications on behalf of the European Geosciences Union.

Abstract

This paper presents the unmanned research aircraft Carolo P360 "ALADINA" (**A**pplication of **L**ight-weight **A**ircraft for **D**etecting **IN**-situ **A**erosol) for investigating the horizontal and vertical distribution of ultrafine particles in the atmospheric boundary layer (ABL). It has a wingspan of 3.6 m, a maximum take-off weight of 25 kg and is equipped with aerosol instrumentation and meteorological sensors. A first application of the system, together with the unmanned research aircraft MASC (Multi-Purpose Airborne Carrier) of the Eberhard-Karls University of Tübingen (EKUT), is described. As small payload for ALADINA, two condensation particle counters (CPC) and one optical particle counter (OPC) were miniaturized by re-arranging the vital parts and composing them in a space saving way in the front compartment of the airframe. The CPCs are improved concerning the lower detection threshold and the response time. Each system was characterized in the laboratory and calibrated with test aerosols. The CPCs are operated with two different lower detection threshold diameters of 6 and 18 nm. The amount of ultrafine particles, which is an indicator for new particle formation, is derived from the difference in number concentrations of the two CPCs. Turbulence and thermodynamic structure of the boundary layer are described by measurements of fast meteorological sensors that are mounted at the aircraft nose. A first demonstration of ALADINA and a feasibility study were conducted in Melpitz near Leipzig, Germany, at the Global Atmosphere Watch (GAW) station of the Leibniz Institute for Tropospheric Research (TROPOS) on two days in October 2013. There, various ground-based instruments are installed for long-term atmospheric monitoring. The ground-based infrastructure provides valuable additional background information to embed the flights in the continuous atmospheric context and is used for validation of the airborne results. The development of the boundary layer, derived from backscatter signals of a portable Raman lidar POLLY^{XT}, allows a quick overview of the current vertical structure of atmospheric particles. Ground-based aerosol number concentrations are consistent with the results from flights in heights of a few meters. In addition, a direct comparison of

AMTD
7, 12283–12322, 2014

ALADINA aerosol data and ground-based aerosol data, sampling the air at the same location, shows comparable values. MASC was operated simultaneously with complementary flight patterns. It is equipped with the same meteorological instruments that offer the possibility to determine turbulent fluxes. Therefore additional information about meteorological conditions was collected in the lowest part of the atmosphere. Vertical profiles up to 1000 m altitude indicate a high variability with distinct layers of aerosol especially for the small particles of a few nanometers in diameter. Particle bursts were observed on one day during the boundary layer development in the morning.

1 Introduction

Atmospheric aerosols play an important role in our climate system (Ramanathan et al., 2001) and for human health (Stieb et al., 2002; Davidson et al., 2005). The size distribution of airborne particles varies between 1×10^{-3} and 100 µm in particle diameter (Baltensperger, 1997). A distinction in different modes according to the particle diameter is often used. In this article the term "ultrafine particles" refers to particles in the nucleation mode (diameter < 30 nm). Due to subsequent growth, particles can reach the Aitken mode (diameter 30–100 nm). Larger particles belong to the accumulation mode (diameter 0.1–1 µm) and the coarse mode (diameter > 1 µm) (e.g., Kannosto et al., 2008). With increasing radius particles have the potential to act as cloud condensation nuclei (CCN) and to influence the climate system indirectly (Spracklen et al., 2008). New particle formation (NPF) is caused by nucleation (gas-to particle conversion) and has been observed at various sites and altitudes of the earth's system (Wiedensohler et al., 1996; Weber et al., 1997; Kulmala et al., 2004; Jaatinen et al., 2009). Formation mechanisms and growth rates have been investigated using different platforms (ground, ship and aircraft). Generally the origin and history of air masses play a key role in NPF (e.g., Sorribas et al., 2011). However, it is still not clear which meteorological situation or chemical species are most efficient for particle bursts. Homogeneous and heterogeneous nucleation require a sufficient amount of precursor gases (Kulmala

AMTD
7, 12283–12322, 2014

et al., 2004). The presence of non-volatile vapours is essential for the growth of freshly formed particles. Binary nucleation of water and sulphuric acid needs conditions of low temperature, high relative humidities, aerosol concentrations and high amount of sulphuric acid (Doyle, 1961; Raes et. al, 1992; Kulmala et al., 2000).

The atmospheric boundary layer (ABL) is the lowest part of the troposphere and is influenced by exchange of heat, water vapour, trace gases and aerosols with the surface. Its properties determine the formation, growth and processing of airborne particles. In the ABL stable conditions are frequent during night time and often coupled with a strong temperature inversion. Inversions prevent interactions of air masses with the free troposphere (FT) so that various horizontal layers of aerosols can coexist without vertical mixing. Knowledge of the influence of atmospheric boundary layer development and turbulent mixing on particle bursts is still poor. Bigg (1997) and Nilsson et al. (2001) assumed nucleation due to turbulent mixing processes. Nilsson et al. (2001) concluded entrainment and convection as a cause for nucleation. Stratmann et al. (2003) investigated particle burst events in the residual layer (RL) and mixed layer (ML). Moreover, NPF was observed with increasing turbulence in the RL by Wehner et al. (2010). Enhanced concentrations of ultrafine particles in the morning can be trapped vertically due to the stable boundary layer. During daytime convection leads to turbulent mixing and vertical profiles of aerosol concentrations demonstrate a homogeneous distribution. In addition, Siebert et al. (2004) presented new particle formation near the inversion layer of the ABL. Another study investigated new particle formation related to a nocturnal low-level jet (LLJ), measured with the system ACTOS (Airborne Cloud Turbulence Observation System), installed bellow a tethered-balloon (Siebert et al., 2007). In this study, NPF events were observed in connection with an increase of SO_2 concentrations in the lower part of the jet. However, more information about sources and formation processes of new particle formation within the atmospheric boundary layer is essential to understand the complex developments of aerosols in the atmosphere and has to be implemented in models (Boy et al., 2006). The vertical aerosol distribution is strongly related to the synoptic conditions, the evolution of the ABL (e.g., Harnisch

AMTD
7, 12283–12322, 2014

et al., 2009), the thermodynamic structures and the atmospheric turbulence (Boy et al., 2003). As different processes can be involved in NPF, and subsequent growth out of the gas phase, repeated vertical profiles of the aerosol concentration and size distribution are needed to elucidate the origin of NPF (Hellmuth, 2006). The variability of small particles over large distances has been analysed by networks of ground-based measurement stations (Vana et al., 2004; Wehner et al., 2007) and additionally by aircraft (O'Dowd et al., 2009). In summary, there are many indications that NPF starts in a vertically confined layer around the altitude of the inversion. Nevertheless, the existing data set is still poor and so far a systematic analysis was not possible due to a missing suitable measurement system. Distributions from the surface up to the free troposphere can be measured by in-situ instruments e.g. towers, tethered balloon systems and radiosondes. Manned aircraft measurements offer information about the vertical distribution of aerosols for larger scales and higher altitudes. Airborne measurements investigated the large scale variability of the particle concentrations along air mass trajectories (O'Dowd et al., 2009). Here, in particular, is a lack in detailed measurements of the small-scale vertical and horizontal variability which, however, are recommended for the implementation of new particle formation (NPF) in models (Boy et al., 2006).

Unmanned aerial systems (UAS), also called remotely piloted aircraft systems (RPAS), offer a lot of advantages as research platforms and have become increasingly important in the last decade. Some applications can be seen in Clarke et al. (2002); Corrigan et al. (2008) and Bates et al. (2013). The miniaturisation of electronic components allows the implementation of three-dimensional GPS-system (Global Positioning System) and IMU (Inertial Measurement Unit) to record accurate position, attitude, time and speed of the aircraft (van den Kroonenberg et al., 2008). Autopilot control offers the possibility to fly with low cruising speed at constant heights in order to derive turbulent fluxes. Further advantages of small unmanned research aircraft are minimal logistical requirements (e.g. no airport necessary), low costs compared to manned aircraft, high flexibility, the possibility to investigate atmospheric parameters at small scales

AMTD
7, 12283–12322, 2014

and low altitudes, and the potential for application in regions that are too dangerous for manned aircraft. With ALADINA, an efficient and flexible tool is created to study the small-scale horizontal and vertical distribution and variability of aerosols in the size range of 6 nm to 10 µm. Complementary to ground-based monitoring instruments, it provides in-situ measurements of aerosol and meteorological properties at variable altitudes up to 1000 m. ALADINA thus can fill the spatial gap in the atmospheric boundary layer measurements between ground-based instruments, LIDAR (LIght Detection And Ranging) column measurements that usually cover an altitude range above 300 m and measurements at higher altitudes with larger extent provided by manned aircraft.

This article presents the unmanned research aircraft ALADINA and the results of a first application. In Sect. 2, the applied measurement systems and methodology are introduced: The airframe Carolo P360, the ALADINA aerosol payload and its calibration, the meteorological sensors and the data acquisition. Further the aircraft MASC is described. In Sect. 3, the measurement site Melpitz and the first field application are discussed in detail. Finally, a summary of the article and a conclusion concerning the new device ALADINA for aerosol research is provided in Sect. 4.

2 Measurement systems and methodology

2.1 Unmanned research aircraft Carolo P360 "ALADINA"

The Carolo P360 is a pusher aircraft with a large payload bay (0.35 m × 0.31 m × 0.19 m) to carry various instrumentation. In the case of ALADINA, (Fig. 1) the P360 is equipped with meteorological sensors and aerosol instrumentation. The aircraft family "Carolo P360" was developed at the Institute of Aerospace Systems at the Technische Universität Braunschweig (Scholtz et al., 2011). It has a wingspan of 3.6 m and a maximum take-off weight of 25 kg. Save operation is given by wind speed less than 15 $m\,s^{-1}$ and below cloud base. The cruising speed is typically 25 to 28 $m\,s^{-1}$. An electrical propulsion system allows a flight endurance of approximately 40 min. After 20 min for

AMTD
7, 12283–12322, 2014

exchanging battery packs and saving data, the P360 can be operated again. Flight preparation includes charging the batteries, checking the whole system and saving data. A combustion engine is generally compatible with the P360 but is not used for ALADINA in order to reduce vibrations that might disturb the measurements of turbulent fluxes and to make sure that the aerosol sensors are not contaminated with the exhaust from ALADINA. Another advantage of the electrically operated system is keeping the centre of gravity constant. This allows a precise calibration of the angle of attack (van den Kroonenberg et al., 2008) that is necessary for determining accurate wind data. The battery system for the electric motor consists of two battery packs with a combined capacity of about 20 Ah. No additional equipment like a winch system or catapult is necessary for take-off. A landing gear, fixed on the lower fuselage, offers an easy handling during take-off and landing on flat surfaces (e.g. grass, asphalt or snow). The airfield requires a dimension of approximately 60 m x 25 m depending on wind conditions and the pilot's experience.

The meteorological sensors and an aerosol inlet are installed at the front of aircraft nose (Fig. 2). The miniaturised aerosol instrumentation is located in the modular payload bay (Fig. 3) of the aircraft. Also, the data acquisition of ALADINA is installed in the front part and allows real-time data transfer by a telemetry downlink. The total weight of the payload is < 2.8 kg. Every electric subsystem like propulsion, autopilot combined with a manual control unit and aerosol instrumentation together with meteorology measurement unit, GPS and IMU has its own power supply and can be operated stand-alone. ALADINA can be flown automatically by the autopilot ROCS (Research Onboard Computing System) that is provided by the Institute of Flight Mechanics and Control of the University Stuttgart. More information can be taken from Haala et al. (2011) and Wildmann et al. (2014a). This autopilot allows precise measurement flights in the lower ABL over larger distances. ALADINA follows the flight pattern which was sent to the aircraft before take-off by the ground station. Within the telemetry range of 1.5 km, the ground staff is able to follow and monitor the position, attitude and airspeed of the aircraft. Changes of the waypoints and altitudes are possible within that range

AMTD
7, 12283–12322, 2014

and during flights. In principle, ALADINA is able to operate at night equipped with the appropriate lighting upon permission of the local civil aviation authorities (CAA). Operation in precipitation is currently not possible since ALADINA is not rainproof concerning the measurement electronics. In addition, operation in clouds is not allowed by the CAA.

2.2 Aerosol instrumentation

The aerosol instrumentation (Fig. 3) consists of three particle counters and a 3/16″ stainless steel tube with rounded inlet lips as aerosol inlet (Fig. 2, Number 3). One optical particle counter, OPC, (model GT-526, Met One Instruments Inc., Washington, USA) and two condensation particle counters, CPCs, (model 3007, TSI Inc., St Paul, USA) were miniaturized and calibrated in the laboratory at the Leibniz Institute for Tropospheric Research. Weight reduction of the instruments was realized by removing housings, internal batteries and displays of the OPC and the CPCs, as well as using only one pump for both CPCs. The CPCs were calibrated in the laboratory with silver particles of different sizes (Hermann and Wiedensohler, 2001). The counting efficiency and response time of the newly designed CPCs are displayed in Figs. 4 and 5. While the counting efficiency curves show a typical behaviour, the response time is surprisingly fast with < 1.3 s for $t_{10-90\,\%}$ compared to the approximately response time of 9 s stated for the original instrument by the manufacturer. Total particle number concentrations are determined by the CPCs with different lower threshold diameters. The difference between the number concentrations of the two CPCs is an indicator of freshly formed particles. The first CPC (Fig. 3, Number 7) measures the number concentration of particles with diameters between 11 nm and 2 µm (N_{11}), and the second one (Fig. 3, Number 8) the concentration of particles in the range between 18 nm and 2 µm (N_{18}). The aerosol volume flow rate through the CPCs was increased from originally 0.10 to 0.16 L min^{-1} in order to decrease the response time of the CPCs. The increased volume flow rates through the CPCs led to an increasing lower threshold diameter. To counter-act this effect and to derive two different lower threshold diame-

AMTD
7, 12283–12322, 2014

ters, temperature differences between the saturator and condenser inside the CPCs were individually increased using software commands. In order to reach even lower threshold diameters, both CPCs were modified again after the test campaign. Now it is possible to detect particles with a diameter of 6 nm from the first CPC. The OPC (Fig. 3, Number 9) runs with its original pump system and an airflow of 2.83 L min^{-1}. The OPC yields the particle number concentrations in six particle size channels from about 0.3 to 10 µm particle diameter.

2.3 Meteorological sensors and data acquisition

The meteorological sensor package, mounted at the front of the aircraft (Fig. 2), was designed and integrated by the Environmental Physics group of the Eberhard-Karls University of Tübingen (EKUT). It contains a full thermodynamic sensor package with an output of the three-dimensional wind vector, barometric pressure, water vapour content and temperature. In order to measure the three-dimensional wind vector, several sensors are involved: The IMU/GPS system IG-500N by SBG systems delivers information about attitude and velocity in the geodetic coordinate system. A five-hole probe which was designed at the Institute of Fluid Dynamics at the Technische Universität Braunschweig measures the airflow angle and true airspeed. Details about the calibration strategy and airflow retrieval from the five-hole probe, as it is performed in the ALADINA system, is given in Wildmann et al. (2014b). The calculation of the wind vector from all single measurements is described in van den Kroonenberg et al. (2008). With this technique, wind fluctuation of up to 30 Hz can be resolved and the total accuracy of the wind speed measurement was estimated to approximately 0.5 m s^{-1} (van den Kroonenberg et al., 2008). The temperature is simultaneously measured by two fast response sensors: a thermocouple and a fine wire platinum resistance thermometer which are described in detail in Wildmann et al. (2013). A relative humidity sensor of type P14 Rapid (Wildmann et al., 2014c) by Innovative Sensor Technologies is used as a small and light weight solution to measure the water vapour content of the air. The sensor has a specified time response of 1.5 s. Careful post-processing, as pre-

AMTD
7, 12283–12322, 2014

sented in Wildmann et al. (2013), is applied and allows a frequency resolution of up to 3 Hz in the current setup. The central data acquisition system is the airborne meteorological on-board computer (AMOC) that was developed by EKUT in cooperation with the University of Applied Sciences Ostwestfalen-Lippe. All the above described sensors, including the aerosol instrumentation, are connected to AMOC. Input channels are processed and stored to a secure digital memory (SD)–card at a sampling rate of 100 Hz. In addition, data transfer through a 2.4 GHz telemetry downlink allows real-time monitoring of sensor data at a ground station computer with a rate of 1 Hz.

2.4 Unmanned research aircraft MASC

For additional information about turbulence within the atmospheric boundary layer and to obtain a three-dimensional picture of atmospheric processes, a second unmanned research aircraft MASC (Multi-purpose Airborne Sensor Carrier) (Wildmann et al., 2014a) was operated during the first test campaign simultaneously with ALADINA. MASC was developed at the EKUT and carries the same meteorological sensors as ALADINA. Depending on battery and payload, MASC has a take-off weight of 5.0–7.0 kg and a wingspan between 2.6 and 3.4 m. It has payload capabilities of up to 1.5 kg. An electrical propulsion provides a maximum flight endurance of 60 min. Launching is realized by a bungee rope on flat surfaces. A safety pilot is responsible for take-off and landing. Once in the air, the aircraft is controlled by autopilot ROCS (see Sect. 2.1) with a cruising speed of 25 $m\,s^{-1}$. Furthermore, the same data acquisition is used in order to derive meteorological parameters. Turbulent fluxes can be obtained in conditions of quasi stationarity by horizontal flight legs at different altitudes. To obtain statistically relevant data, an average length of at least 1 km is evaluated for each altitude.

AMTD
7, 12283–12322, 2014

3 First field application

3.1 Measurement site and experiment

A feasibility study and test of ALADINA performance were conducted at the research station of TROPOS in Melpitz on 8 and 9 October 2013. The site is settled 41 km north-east of Leipzig, Germany. It is built on a flat meadow and surrounded by agricultural land (Spindler et al., 2013). The surface is smooth and meets the requirements for take-off and landing the aircraft. Air masses are influenced by industrial and agricultural pollution due to the proximity to Leipzig and due to its surrounding of grass, crop land and woods. The measurement site is qualified for networks like European Monitoring and Evaluation Programme (EMEP) and Aerosols, Clouds, and Trace gases Research InfraStructure Network (ACTRIS). Ground based instruments are used for long-term monitoring in Melpitz. In addition to meteorological parameters, gas concentrations (for example O_3, NO, NO_2 and SO_2) and atmospheric aerosols are analysed. Particle number size distributions are measured in a range between 5 and 800 nm by a twin scanning mobility particle sizer (TSMPS) system (Jaatinen et al., 2009; Wiedensohler et al., 2012). Larger particles are detected by an aerodynamic particle sizer (APS). Scans are performed every 10 min and offer the possibility to observe the temporal development of the atmospheric aerosol. Apart from this, optical instruments detect scattering and absorption coefficients in order to investigate the optical particle properties. The portable 3 + 2 Raman lidar POLLY^{XT} (Althausen et al., 2009) was operated at the same time in Melpitz. The data set obtained during the field campaign is used in order to describe the boundary layer development. Previous studies reveal that the station offers great potential for detecting formation mechanisms of ultrafine particles. New particle formation has been mostly observed during spring and summer with particle size distributions increasing from sunrise to noon (Birmili and Wiedensohler, 2000; Birmili et al., 2001). Jaatinen et al. (2009) investigated new particle formation events at three different European sites including Melpitz. Long-term measurements for two years (July 2003–June 2005) show nucleation events depending on seasons. Opera-

AMTD
7, 12283–12322, 2014

tional data implies that 26 % of all measurement days contain events with new particle formation. Formation rates of up to 4.6 $cm^{-3} s^{-1}$ in polluted air masses were detected. Furthermore a mean growth rate of 6.1 $nm\,h^{-1}$ was determined.

ALADINA was operated during three measurement flights in October 2013. Due to technical problems during the first flight, only the data sets obtained during the second and third flight are analysed here. Flight two lasted from 13:05 to 13:35 UTC on 8 October 2013. The measurement period of flight three took place from 08:26 to 08:58 UTC on 9 October 2013. Altogether, it was possible to obtain 14 vertical profiles with varying vertical extent (0–1000 m, 100–500 or less maximum altitude). During the test campaign, combined flights with the two research aircraft ALADINA and MASC were performed. Each flight consisted of several vertical profiles from the surface up to 1000 m and horizontal legs at various altitudes to investigate layers of enhanced aerosol concentrations and to observe the horizontal distribution of atmospheric aerosols. The best strategy resulted to be vertical profiling of ALADINA, to catch the development of the ABL and to observe the vertical distribution of aerosols, while MASC performed measurements of turbulent fluxes at the interesting altitudes (for example below and above the inversion or at the layers of enhanced aerosol concentration).

In the following, the general synoptic situation and the meteorological parameters, that were recorded at the observatory during the field campaign, are presented so that one may gets an overview of the prevailing weather condition (Sect. 3.2). Data sets obtained by the lidar POLLY^{XT} and by vertical soundings with the research aircraft ALADINA and MASC, are discussed in the context of the boundary layer development on the two measurement days (Sect. 3.3). Aerosol variability, depending on diurnal cycles at the ground, is shown by data sets of a TSMPS and finally compared with the vertical profiling of ALADINA in two different case studies (Sect. 3.4).

3.2 Synoptic situation

In this subsection, the weather situation is described in order to obtain information about the contribution of air masses that arrived at the measurement site during the

AMTD
7, 12283–12322, 2014

field campaign in October. First, the general weather situation is analysed by the 500 hPa geopotential height, derived from the GFS model on 8 October at 12:00 UTC (Fig. 6a). Air masses in Melpitz are influenced by a high pressure system at the surface above eastern Germany. In the 500 hPa geopotential level, a trough leads to cold advection in the atmosphere. Due to the presence of the high pressure system in the lower part of the atmosphere, the trough has been weaken. The wave system moves eastwards which can be seen by a comparison of the general weather situation with the next day. Figure 6b reveals the general synoptic situation on 9 October at 08:00 UTC. Middle Europe is still influenced by a high pressure system at the surface. The trough, which is developing over the Atlantic Ocean in northern Europe, has been settled further to Great Britain. All in all, the weather situation in Germany is rather stable. Back trajectories indicate the source and transport of air masses and were generated by using the NOAA Hysplit model (Draxler and Rolph, 2014; Rolph, 2014). In this case, we used the back trajectories in the heights of 500, 1000 and 1500 m in order to describe their origin and long-transport within the ABL (Fig. 6c). Analysis of back trajectories reveal the origin of air masses over the Atlantic Ocean. Furthermore, air masses are transported south-west over the northern part of Great Britain and western part of Germany before reaching the research site in Melpitz on 9 October at 08:00 UTC. Especially the back trajectory of 500 m shows a longer residence time of two days over the eastern part of Germany. However, we assume rather clean air with low concentrations of atmospheric aerosols because the air masses are mainly influenced by marine environmental conditions. In order to describe the detailed weather situation on-site, we use the meteorological data that was measured continuously by a weather mast at the research station in 1 and 6 m height above ground during the flights period. On 8 October (Fig. 7), the temperature range in 1 m level is between 4.9 °C at 22:10 UTC and 18 °C at 13:55 UTC. The relative humidity reaches a maximum value of 99 % in the morning and in the evening at 19:40 UTC. Nevertheless, no rain was measured by the sensor. The pressure decreases continuously from 1017 to 1013 hPa during the day. The main wind direction is north-east but the wind is changing from north to south-

AMTD
7, 12283–12322, 2014

west in the afternoon. The maximum wind speed of 3 m s^{-1} is detected in 6 m above ground at 14:30 UTC. Fluctuations of global radiation values indicate a continuously changing cloud coverage. During the second flight time (13:05–13:35 UTC), the temperature reaches values of 16.5–17.6 °C. The relative humidity varies between 55 and 59 % with a pressure of 1014 hPa. The wind is weak with a maximum of 1.9 m s^{-1} and from north-east. The global radiation ranges from 448 to 533 W m^{-2}. Figure 8 shows the situation for the third flight on 9 October. The pressure decreases further from 1013 to 999 hPa during the day. The temperature reaches values up to 17.2 °C at 10:05 UTC and a minimum of 8.8 °C at 06:00 UTC. Again, the humidity shows the dependency on temperature. Maximum values are in the morning and night. During day, the relative humidity reaches rather dry conditions of 60 %. The wind speed gains up to 4.2 m s^{-1} and the wind direction is changing to south-west. During flight time (08:26–08:58 UTC), the pressure is 1009 hPa and the temperature is in a range of 14.3 and 16.8 °C. The relative humidity is rather constant with values around 73 % and the wind speed reaches a maximum of 3.3 m s^{-1} from south to south-west. Further fluctuations of the global radiation are an indicator for a changing cloud coverage. Here, the values of the global radiation are 300–515 W m^{-2} during the third flight of ALADINA.

3.3 Boundary layer development

First, the boundary layer development is analysed by the data set of the lidar POLLY^{XT} (Figs. 9 and 10) that was installed at the same time in Melpitz. Lidar backscatter profiles reveal a boundary layer with pronounced aerosol load indicated by green, yellow and red colours. Figure 9 represents the backscatter signal in the 532 nm range depending on height from 100 m up to 2 km on 8 October 2013. A strong inversion layer was present in the morning, increasing from about 800 to 1100 m altitude. At this height, clouds were formed which can be identified by white structures in the lidar POLLY^{XT} backscatter profiles. The clouds dissolved during the midday and afternoon. All in all, backscatter signals indicate a well-mixed contribution within the ABL. Figure 11 shows

AMTD
7, 12283–12322, 2014

seven vertical profiles of potential temperature (Fig. 11a) and mixing ratio (Fig. 11b) obtained by vertical sounding of ALADINA and combined with MASC on 8 October. The first two profiles at 08:59 and 09:04 UTC were flown with MASC and demonstrate a well-mixed ABL up to an altitude of 500 m a.g.l. The potential temperature gradient is stable by values of 268.5 to 287.0 K within the two profiles. Following profiles show still a well-mixed ABL with no significant inversion layer. During ALADINA flights at 13:05, 13:14 and 13:18 UTC, the ABL topping inversion was higher than the maximum flight altitude of 1000 m a.g.l. The last profile of MASC at 15:01 UTC indicates a weak inversion at 300 m. On this day, the mixing ratio obtained by the profiles of both aircraft varies between 6.6 and 8.4 $g\,kg^{-1}$ at the surface and decreasing values with height.

On 9 October, the ABL is composed of two different air masses which can be seen by the backscatter signal in Fig. 10. Starting from the surface at night, the layer extends to approximately 400 m a.g.l. at 08:00 UTC due to solar radiation and therefore given by the exchange of heat fluxes at the surface. During the day, the second layer is still increasing and finally mixed within the ABL at 14:00 UTC in the afternoon. Again, vertical profiles of both UAS are used in order to describe the lower part of the ABL in a range of 0–1000 m altitude in detail (Fig. 12). Three vertical profiles were flown with ALADINA from 08:26 to 08:41 UTC with various vertical extend. Thereafter one vertical profile of MASC ranged from 150 to 650 m a.g.l. at 08:58 UTC. The mixing ratio reaches values up to 9 $g\,kg^{-1}$ at the surface and the potential temperature a minimum of 288 K at 150 m a.g.l. Above 350 m a different layer with other properties, almost neutrally stratified, extends up to 750 m which can be taken from both parameters.

3.4 Aerosol distribution within the ABL

During the campaign in October 2013, the aerosol number concentration of particles larger than 10 nm varied between 1500 and 35 500 cm^{-3} (Figs. 13 and 14) which is relatively low for continental conditions. But as it was mentioned in Sect. 3.2, the origin of air masses was over the Atlantic Ocean. Furthermore, air masses were transported

AMTD
7, 12283–12322, 2014

only within the last two days over Central Europe so that there was a low potential for pollution.

On 8 October, the contour plot obtained by the TSMPS data (Fig. 13) shows a significant decrease of the number concentrations between less than 1600 and 4470 cm^{-3} within the developing boundary layer around 07:00 UTC. At 10:00 UTC, an increase of particle number concentrations with a diameter of about 10 nm is observed and meets a maximum of 35 000 cm^{-3}. These small particles are formed due to new particle formation. At 11:00 UTC, a particle burst of aerosols with a diameter range of 100 to 200 nm occurs. After 12:00 UTC the picture appears even more variable. NPF stops and starts again but with a broader burst. This is probably due to variations in the global radiation by increasing coverage of cumulus clouds (see Fig. 7). However, this day is not a classical new particle formation day with a continuous growth of the small particles, they appear as small bursts. These ground-based measurements fit well with the measured profiles of ALADINA. A continuous difference between CPC1 and CPC2 is observed (Fig. 15c), meaning there is a significant number of particles in the size range between 11 and 18 nm. On the next day (9 October), no sharp jump of number concentrations of small particles with a diameter of 10 nm can be observed by the TSMPS at the ground (Fig. 14). But the total aerosol number concentration is increasing and maximum values of 35 500 cm^{-3} with a diameter range of 30 to 100 nm occur at 11:30 UTC. Compared to the day before, the variability of atmospheric aerosols is more homogeneous. This is consistent with the results of the third flight of ALADINA at 08:37 UTC. The number concentration of small particles is increasing at the ground to a maximum of 17 000 cm^{-3} (Fig. 16c). Both CPCs measure the same number concentrations, except in one layer between 500 and 600 m a.g.l. This is obviously the only region with a significant number concentration of small particles. Here, a high dependency of atmospheric aerosols on the atmospheric stratification can be observed. Even larger particles (300 to 700 nm in diameter), measured by the OPC, show a similar behaviour.

AMTD
7, 12283–12322, 2014

According to the time series of the backscatter lidar POLLY^{XT} (Fig. 9), the ABL altitude increases from about 800 m above ground to about 1100 m during the morning transition on 8 October. The aerosol load appears to be rather well-mixed within the ABL because no strong layers could be identified from the colour scheme. On 9 October, an increase of the ABL altitude from about 1000 to 1200 m is also observed (Fig. 10). The aerosol distribution shows a layer of clearly enhanced aerosol load at an altitude below 400 m. These features are in agreement with the observations of ALADINA. In Figs. 15d and 16d the profiles of the OPC 0.5 µm channel reveal a uniform distribution of aerosols up to 1000 m on 8 October. In contrast, an enhanced aerosol load in the lowermost 400 m is observed on 9 October. Both days indicate clean air masses due to the small amount of atmospheric particles with a diameter range of larger than 300 nm. However, for the small particles recorded with the CPCs, there is an additional fine layer structure visible that is not caught by the larger wavelengths of the OPC (300, 500 and 700 nm). On 8 October, layers with enhanced small particle concentration are observed directly above ground, at an altitude of 200 to 250 and at 600 m. All in all, a high vertical variability of the small-size aerosol concentration is presented (Fig. 15c). On 9 October 2013, the small-size particles are also enhanced in the lowest 320 m. Pronounced peaks of small-size aerosol are found at an altitude of 650 and 780 m. The enhanced aerosol load in the lowest 400 m on 9 October 2013 is directly related to the ABL conditions. The profile of the potential temperature (Fig. 16a) shows a slightly unstable stratification within the lowermost 400 m. At this altitude, a shallow layer of stably stratified air prevents mixing with higher altitudes. Also, the mixing ratio is considerably enhanced in the lowest 400 m (Fig. 16b). From 320 to 870 m the thermal profile is neutral and then again stable above. The layer of enhanced small-size aerosol concentration at 780 m coincides with the beginning of the stable stratification. In contrast, the profile of the potential temperature on 8 October reveals an almost neutral, but strongly varying potential temperature (Fig. 15a). This indicates that air masses of different origin might have been sampled during the ascent of ALADINA in spirals. Again, the layers of enhanced small size aerosol concentration (Fig. 15c) coincide with

AMTD
7, 12283–12322, 2014

the altitudes where changes in the profile of the potential temperature are observed, enabling or prohibiting mixing processes.

4 Summary and conclusions

In this study, the new unmanned research aircraft Carolo P360 "ALADINA" is presented. It was developed for atmospheric boundary layer aerosol research and thus equipped with a small and light (< 2.8 kg) aerosol and meteorological payload. Two CPCs (condensation particle counters) with different threshold diameters (11 and 18 nm) offer the possibility to measure total particle number concentrations of freshly formed particles. An OPC (optical particle counter) records size distributions of larger particles in six channels between 0.3 and 10 µm. Fast meteorological sensors with a resolution of up to 30 Hz provide turbulence measurements and thus the possibility to connect atmospheric and aerosol dynamics. After sensor characterization in the laboratory and in a wind tunnel, a first test campaign was conducted at the GAW station Melpitz (Germany) in October 2013. Typical flight patterns for identifying the vertical distribution of aerosols were flown by vertical profiles from the ground up to 1000 m altitude. Additionally, MASC provided measurements of meteorological parameters simultaneously. In this paper, data of two flights with different aerosol conditions were analyzed. One flight was performed on a day with new particle formation and one flight where no new particle formation event was observed at the ground, but an internal layer in the atmospheric boundary layer with different aerosol properties was present. The comparison of the ALADINA results with ground-based in-situ aerosol instruments and a lidar POLLY^{XT} gives confidence in the obtained data and in the capability of this new system to record aerosol size distributions with good reliability. After the campaign, one additional original TSI Peltier element was installed to cool the condenser of one CPC and to increase the temperature difference inside the second CPC to achieve two more distinct detection threshold limits (6 and 18 nm). The potential of this flexible airborne system for new particle formation investigations will be further explored in

AMTD
7, 12283–12322, 2014

future follow-up campaigns at the Melpitz observatory. The further technical and scientific development of ALADINA will accompany the follow-up campaigns. The possibility to optionally implement other aerosol instruments (e.g. an aethalometer) is currently under discussion. Future applications will also include the validation of remote sensing derived aerosol properties.

Acknowledgements. This work is supported by the German Research Foundation (LA 2907/5-1, WI 1449/22-1, BA 1988/14-1). We thank Gerald Lohmann for his contribution with setting up ALADINA. Thanks to the aerosol and lidar groups of TROPOS for using the ground-based data of the research station and for organizing the radiosonde ascent. A special thanks to Achim Grüner, Chemistry Department, for technical assistance during the campaign. The authors acknowledge Lutz Bretschneider and Philipp Schrapel for the implementation as good safety pilots. We thank the local aviation authorities for support with the flight permission.

References

Althausen, D., Engelmann, R., Baars, H., Heese, B., Ansmann, A., Müller, D., and Komppula, M.: Portable Raman Lidar Polly^{XT} for automated profiling of aerosol backscatter, extinction, and depolarization, J. Atmos. Ocean. Tech., 26, 2366–2378, 2009. 12293

Baltensperger, U.: Analysis of aerosols, Chimia, 51, 686–689, 1997. 12285

Bates, T. S., Quinn, P. K., Johnson, J. E., Corless, A., Brechtel, F. J., Stalin, S. E., Meinig, C., and Burkhart, J. F.: Measurements of atmospheric aerosol vertical distributions above Svalbard, Norway, using unmanned aerial systems (UAS), Atmos. Meas. Tech., 6, 2115–2120, doi:10.5194/amt-6-2115-2013, 2013. 12287

Bigg, E. K.: A mechanism for the formation of new particles in the atmosphere, Atmos. Res., 43, 129–137, 1997. 12286

Birmili, W. and Wiedensohler, A.: New particle formation in the continental boundary layer: Meteorological and gas phase parameter influence, Geophys. Res. Lett., 27, 3325–3328, 2000. 12293

Birmili, W., Wiedensohler, A., Heintzenberg, J., and Lehmann, K.: Atmospheric particle number size distribution in central Europe: Statistical relations to air masses and meteorology, J. Geophys. Res., 106, 32005–32018, 2001. 12293

AMTD

7, 12283–12322, 2014

Boy, M., Rannik, Ü., Lehtinen, K. E. J., Tarvainen, V., Hakola, H., and Kulmala, M.: Nucleation events in the continental boundary layer: Long-term statistical analyses of aerosol relevant characteristics, J. Geophys. Res., 108, 4667, doi:10.1029/2003JD003838, 2003. 12287

Boy, M., Hellmuth, O., Korhonen, H., Nilsson, E. D., ReVelle, D., Turnipseed, A., Arnold, F., and Kulmala, M.: MALTE – model to predict new aerosol formation in the lower troposphere, Atmos. Chem. Phys., 6, 4499–4517, doi:10.5194/acp-6-4499-2006, 2006. 12286, 12287

Clarke, A. D., Ahlquist, N. C., Howell, S., and Moore, K.: A miniature optical particle counter for in situ aircraft aerosol research, J. Atmos. Ocean. Tech., 19, 1557–1566, 2002. 12287

Corrigan, C. E., Roberts, G. C., Ramana, M. V., Kim, D., and Ramanathan, V.: Capturing vertical profiles of aerosols and black carbon over the Indian Ocean using autonomous unmanned aerial vehicles, Atmos. Chem. Phys., 8, 737–747, doi:10.5194/acp-8-737-2008, 2008. 12287

Davidson, C. I., Phalen, R. F., and Solomon, P. A.: Airborne particulate matter and human health: a review, Aerosol Sci. Tech., 39, 736–749, doi:10.1080/02786820500191348, 2005. 12285

Doyle, G. J.: Self-nucleation in the sulphuric acid-water system, J. Chem. Phys., 35, 795–799, 1961. 12286

Draxler, R. R. and Rolph, G. D.: HYSPLIT (HYbrid Single-Particle Lagrangian Integrated Trajectory) Model access via NOAA ARL READY Website, available at: http://ready.arl.noaa.gov/HYSPLIT.php (last access: 8 October 2013), NOAA Air Resources Laboratory, Silver Spring, MD, 2014. 12295

Haala, N., Cramer, M., Weimer, F., and Trittler, M.: Performance test on UAV-based photogrammetric data collection, in: Proceedings of the International Archives of the Photogrammetry, Remote Sensing and Spatial Information Sciences, Zurich, Switzerland, 14–16 September 2011, XXXVIII-1/C22, 7–12, 2011. 12289

Harnisch, F., Gohm, A., Fix, A., Schnitzhofer, R., Hansel, A., and Neininger, B.: Spatial distribution of aerosols in the Inn Valley atmosphere during wintertime, Meteorol. Atmos. Phys., 103, 223–235, 2009. 12286

Hermann, M. and Wiedensohler, A.: Counting efficiency of condensation particle counters at low-pressures with illustrative data from the upper troposphere, J. Aerosol Sci. 32, 975–991, 2001. 12290

Hellmuth, O.: Columnar modelling of nucleation burst evolution in the convective boundary layer – first results from a feasibility study – Part III: Preliminary results on physicochemical model

AMTD
7, 12283–12322, 2014

performance using two “clean air mass” reference scenarios, Atmos. Chem. Phys., 6, 4231–4251, doi:10.5194/acp-6-4231-2006, 2006. 12287

Jaatinen, A., Hamed, A., Joutsensaari, J., Mikkonen, S., Birmili, W., Wehner, B., Spindler, G., Wiedensohler, A., Decesari, S., Mircea, M., Faccini, M. C., Junninen, H., Kulmala, M., Lehtinen, K. E. J., and Laaksonen, A.: A comparison of new particle formation events in the boundary layer at three different sites in Europe, Boreal Environ. Res., 14, 481–498, 2009. 12285, 12293

Kannosto, J., Virtanen, A., Lemmetty, M., Mäkelä, J. M., Keskinen, J., Junninen, H., Hussein, T., Aalto, P., and Kulmala, M.: Mode resolved density of atmospheric aerosol particles, Atmos. Chem. Phys., 8, 5327–5337, doi:10.5194/acp-8-5327-2008, 2008. 12285

Kulmala, M., Pirjola, L., and Mäkelä, J. M., and Jyrki, M.: Stable sulphate clusters as a source of new atmospheric particles, Nature, 404, 66–69, 2000. 12286

Kulmala, M., Vehkamäki, H., Petäjä, T., Dal Maso, M., Lauri, A., Kerminen, V.-M., Birmili, W., and McMurry, P. H.: Formation and growth rates of ultrafine atmospheric particles: a review of observations, Aerosol Sci., 35, 143–176, 2004. 12285

Nilsson, E. D., Rannik, Ü., Kulmala, M., Buzorius, G., and O’Dowd, C. D.: Effects of continental boundary layer evolution, convection, turbulence and entrainment, on aerosol formation, Tellus, 53, 441–461, 2001. 12286

O’Dowd, C. D., Yoon, Y. J., Junkermann, W., Aalto, P., Kulmala, M., Lihavainen, H., and Viisanen, Y.: Airborne measurements of nucleation mode particles II: boreal forest nucleation events, Atmos. Chem. Phys., 9, 937–944, doi:10.5194/acp-9-937-2009, 2009. 12287

Raes, F., Saltelli, A., and Van Dingenen, R.: Modelling formation and growth of H_2SO_4-H_2O aerosols: Uncertainty analysis and experimental evaluation, J. Aerosol Sci., 23, 759–771, 1992. 12286

Ramanathan, V., Crutzen, P. J., Kiehl, J. T., and Rosenfeld, D.: Aerosols, climate, and the hydrological cycle, Science, 294, 2119–2124, 2001. 12285

Rolph, G. D.: Real-time Environmental Applications and Display sYstem (READY) Website, available at: http://ready.arl.noaa.gov (last access: 8 October 2013), NOAA Air Resources Laboratory, Silver Spring, MD, 2014. 12295

Scholtz, A., Kaschwich, C., Krüger, T., Kufieta, K., Schnetter, P., Wilkens, C.-S., and Vörsmann P.: Development of a new multi-purpose UAS for scientific application, in: Proceedings of the International Conference on Unmanned Aerial Vehicle in Geomatics (UAV-g), Zurich, Switzerland, 14–16 September 2011, XXXVIII-1/C22, 149–154, 2011. 12288

AMTD
7, 12283–12322, 2014

Siebert, H., Stratmann, F., and Wehner, B.: First observations of increased ultrafine particle number concentrations near the inversion of a continental planetary boundary layer and its relation to ground-based measurements, Geophys. Res. Lett., 31, L09102, doi:10.1029/2003GL019086, 2004. 12286

Siebert, H., Wehner, B., Hellmuth, O., Stratmann, F., Boy, M., and Kulmala, M.: New particle formation in connection with a nocturnal low-level jet: Observations and modeling results, Geophys. Res. Lett., 34, L16822, doi:10.1029/2007GL029891, 2007. 12286

Sorribas, M., de la Morena, B. A., Wehner, B., López, J. F., Prats, N., Mogo, S., Wiedensohler, A., and Cachorro, V. E.: On the sub-micron aerosol size distribution in a coastal-rural site at El Arenosillo Station (SW – Spain), Atmos. Chem. Phys., 11, 11185–11206, doi:10.5194/acp-11-11185-2011, 2011. 12285

Spindler, G., Grüner A., Müller K., Schlimper, S., and Herrmann, H.: Long-term size-segregated particle (PM_{10}, $PM_{2.5}$, PM_1) characterization study at Melpitz–influence of air mass inflow, weather conditions and season, J. Atmos. Chem., 70, 2, 165–195, 2013. 12293

Spracklen, D. V., Carslaw, K. S., Kulmala, M., Kerminen, V.-M., Sihto, S.-L., Riipinen, I., Merikanto, J., Mann, G. W., Chipperfield, M. P., Wiedensohler, A., Birmili, W., and Lihavainen, H.: Contribution of particle formation to global cloud condensation nuclei concentrations, J. Geophys. Res., 35, L06808, doi:10.1029/2007GL033038, 2008. 12285

Stieb, D. M., Judek, S., and Burnett, R. T.: Meta-analysis of time-series studies of air pollution and morality: effects of gases and particles and their influence of cause of death, age and season, Journal of Air and Management Association, 52, 470–484, 2002. 12285

Stratmann, F., Siebert, H., Spindler, G., Wehner, B., Althausen, D., Heintzenberg, J., Hellmuth, O., Rinke, R., Schmieder, U., Seidel, C., Tuch, T., Uhrner, U., Wiedensohler, A., Wandinger, U., Wendisch, M., Schell, D., and Stohl, A.: New-particle formation events in a continental boundary layer: first results from the SATURN experiment, Atmos. Chem. Phys., 3, 1445–1459, doi:10.5194/acp-3-1445-2003, 2003. 12286

van den Kroonenberg, A., Martin, T., Buschmann, M., Bange, J., and Vörsmann, P.: Measuring the wind vector using the autonomous mini aerial vehicle M^2AV, J. Atmos. Ocean. Tech., 25, 1969–1982, 2008. 12287, 12289, 12291

Vana, M., Kulmala, M., Dal Maso, M., Hõrrak, U., and Tamm, E.: Comparative study of nucleation mode aerosol particles and intermediate air ions formation events at three sites, J. Geophys. Res., 109, D17201, doi:10.1029/2003JD004413, 2004. 12287

AMTD
7, 12283–12322, 2014

Weber, R. J., Marti, J. J., McMurry, P. H., Eisele, F. L., Tanner, D. J., and Jefferson, A.: Measurements of new particle formation and ultrafine particle growth rates at clean continental site, J. Geophys. Res., 102, 4375–4385, 1997. 12285

Wehner, B., Siebert, H., Stratmann, F., Tuch, T., Wiedensohler, A., Petäjä, T., Dal Maso, M., and Kulmala, M.: Horizontal homogeneity and vertical extent of new particle formation events, Tellus B, 59, 362–371, 2007. 12287

Wehner, B., Siebert, H., Ansmann, A., Ditas, F., Seifert, P., Stratmann, F., Wiedensohler, A., Apituley, A., Shaw, R. A., Manninen, H. E., and Kulmala, M.: Observations of turbulence-induced new particle formation in the residual layer, Atmos. Chem. Phys., 10, 4319–4330, doi:10.5194/acp-10-4319-2010, 2010. 12286

Wiedensohler, A., Covert, D. S., Swietlicki, E., Aalto, P., Heintzenberg, J., and Leck, C.: Occurrence of an ultrafine particle mode less than 20 nm diameter in the marine boundary layer during Arctic summer and autumn, Tellus, 48, 213–222, 1996. 12285

Wiedensohler, A., Birmili, W., Nowak, A., Sonntag, A., Weinhold, K., Merkel, M., Wehner, B., Tuch, T., Pfeifer, S., Fiebig, M., Fjäraa, A. M., Asmi, E., Sellegri, K., Depuy, R., Venzac, H., Villani, P., Laj, P., Aalto, P., Ogren, J. A., Swietlicki, E., Williams, P., Roldin, P., Quincey, P., Hüglin, C., Fierz-Schmidhauser, R., Gysel, M., Weingartner, E., Riccobono, F., Santos, S., Grüning, C., Faloon, K., Beddows, D., Harrison, R., Monahan, C., Jennings, S. G., O'Dowd, C. D., Marinoni, A., Horn, H.-G., Keck, L., Jiang, J., Scheckman, J., McMurry, P. H., Deng, Z., Zhao, C. S., Moerman, M., Henzing, B., de Leeuw, G., Löschau, G., and Bastian, S.: Mobility particle size spectrometers: harmonization of technical standards and data structure to facilitate high quality long-term observations of atmospheric particle number size distributions, Atmos. Meas. Tech., 5, 657–685, doi:10.5194/amt-5-657-2012, 2012. 12293

Wildmann, N., Mauz, M., and Bange, J.: Two fast temperature sensors for probing of the atmospheric boundary layer using small remotely piloted aircraft (RPA), Atmos. Meas. Tech., 6, 2101–2113, doi:10.5194/amt-6-2101-2013, 2013. 12291, 12292

Wildmann, N., Hofsäß, M., Weimer, F., Joos, A., and Bange, J.: MASC – a small Remotely Piloted Aircraft (RPA) for wind energy research, Adv. Sci. Res., 11, 55–61, doi:10.5194/asr-11-55-2014, 2014a. 12289, 12292

Wildmann, N., Ravi, S., and Bange, J.: Towards higher accuracy and better frequency response with standard multi-hole probes in turbulence measurement with remotely piloted aircraft (RPA), Atmos. Meas. Tech., 7, 1027–1041, doi:10.5194/amt-7-1027-2014, 2014b. 12291

AMTD
7, 12283–12322, 2014

Wildmann, N., Kaufmann, F., and Bange, J.: An inverse-modelling approach for frequency response correction of capacitive humidity sensors in ABL research with small remotely piloted aircraft (RPA), Atmos. Meas. Tech., 7, 3059–3069, doi:10.5194/amt-7-3059-2014, 2014. 12291

AMTD
7, 12283–12322, 2014

Figure 1. ALADINA during a measurement flight.

AMTD
7, 12283–12322, 2014

Figure 2. The meteorological payload is mounted at the tip of the aircraft. The components are: (1) five-hole probe, (2) temperature sensor (thermocouple) and humidity sensor P14 Rapid, (3) aerosol inlet, (4) fine wire platinum resistance thermometer, (5) GPS antenna and (6) telemetry antenna for real-time data transfer.

AMTD
7, 12283–12322, 2014

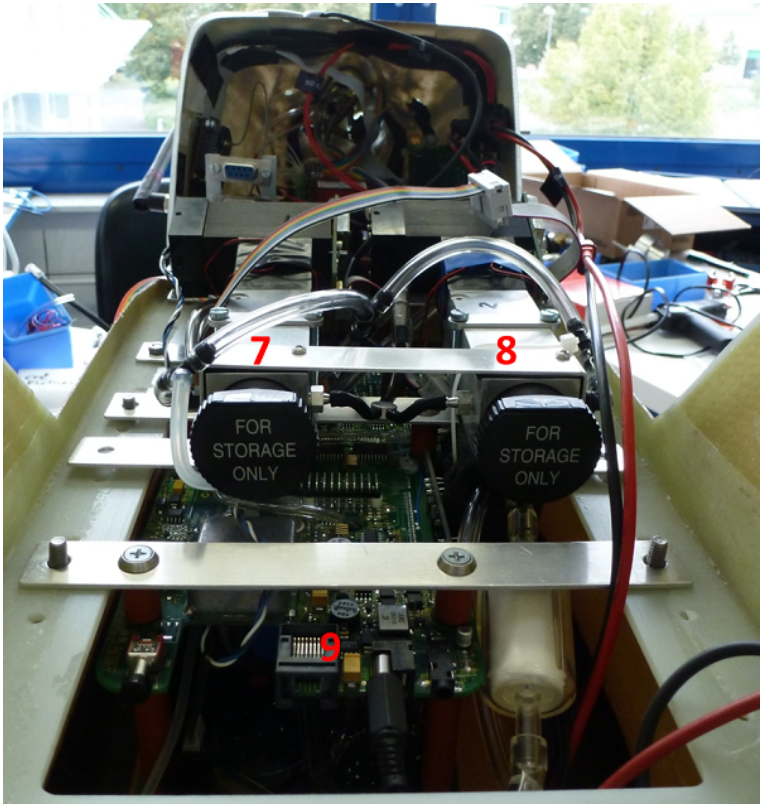

Figure 3. The aerosol payload is installed in the front compartment of the air plane and consists of two condensation particle counters (7 and 8) and one optical particle counter (9) that is mounted underneath (view from the rear). The first CPC1 (7) detects particle number concentrations in a particle diameter range of 11 nm to 2 µm. The second CPC2 (8) measures the particle number concentrations between 18 nm and 2 µm.

AMTD
7, 12283–12322, 2014

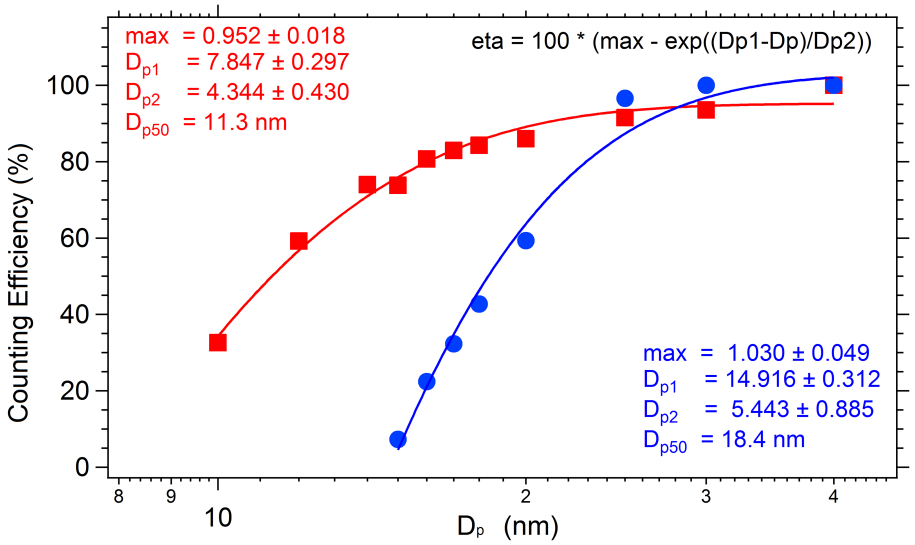

Figure 4. The counting efficiency of the CPCs with different detection limits (11 and 18 nm, respectively) depending on the particle diameter (D_p). The difference between the readings of the two CPCs provides the number concentration of ultrafine particles that are an indicator for new particle formation.

AMTD
7, 12283–12322, 2014

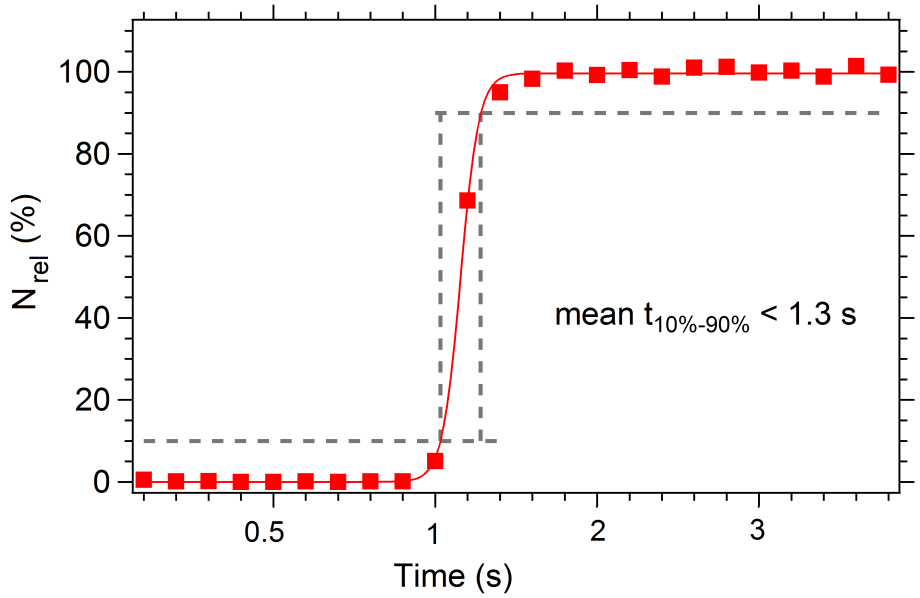

Figure 5. The mean response time of 1.3 s was initiated by a high increase in number concentration that is represented by the relative number concentration (N_{rel}) during a calibration in the laboratory.

AMTD
7, 12283–12322, 2014

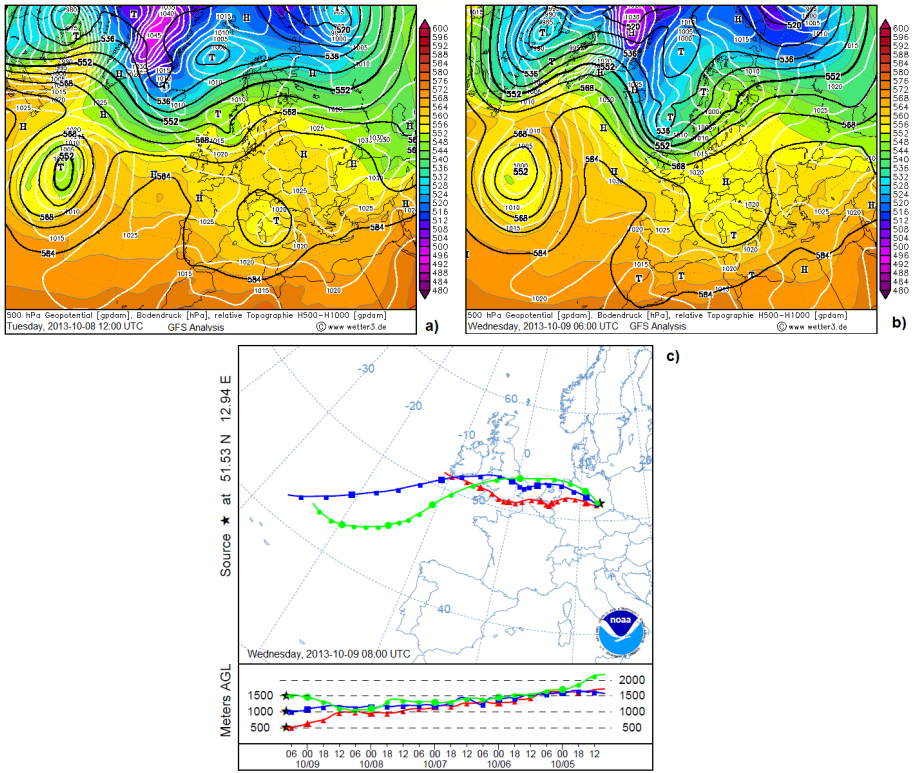

Figure 6. (a) GFS-analysis of the geopotential height in 500 hPa-level, surface pressure and temperature on 8 October 2013 at 12:00 UTC, **(b)** the same as **(a)** but on 9 October 2013 at 06:00 UTC, **(c)** back trajectory in Melpitz on 9 October 2013 at 08:00 UTC, created with the NOAA Hysplit model.

AMTD
7, 12283–12322, 2014

ALADINA – unmanned aircraft for detecting ultrafine particles in the boundary layer

B. Altstädter et al.

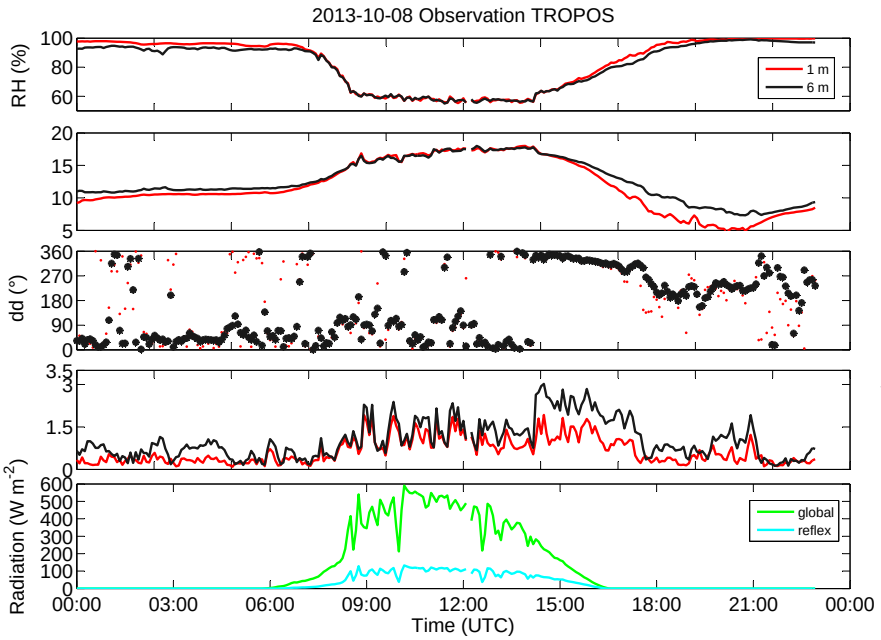

Figure 7. Meteorological parameters at the research site in Melpitz on 8 October 2013. The depicted time range is from 00:00 to 22:50 UTC with 5 min intervals. The data contains measurements of relative humidity (RH), temperature (*T*), wind direction (dd) and wind speed (ff) in the height of 1 m (red line, red stars) and 6 m (black line, black dots) above ground. Further global solar radiance (green line) and reflected global radiation (blue line) are recorded in the short-wave range.

AMTD
7, 12283–12322, 2014

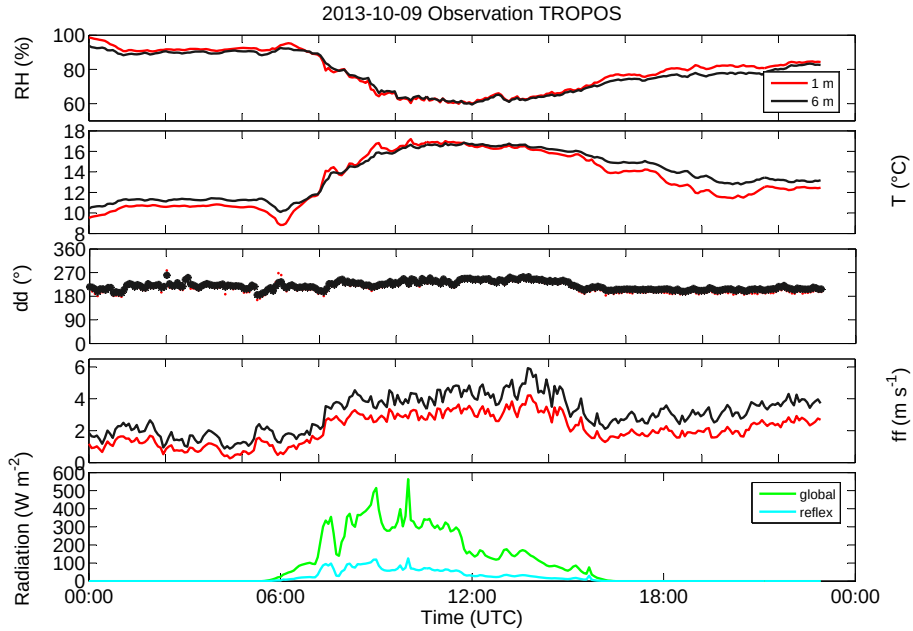

Figure 8. Same as Fig. 7 but on 9 October 2013.

AMTD
7, 12283–12322, 2014

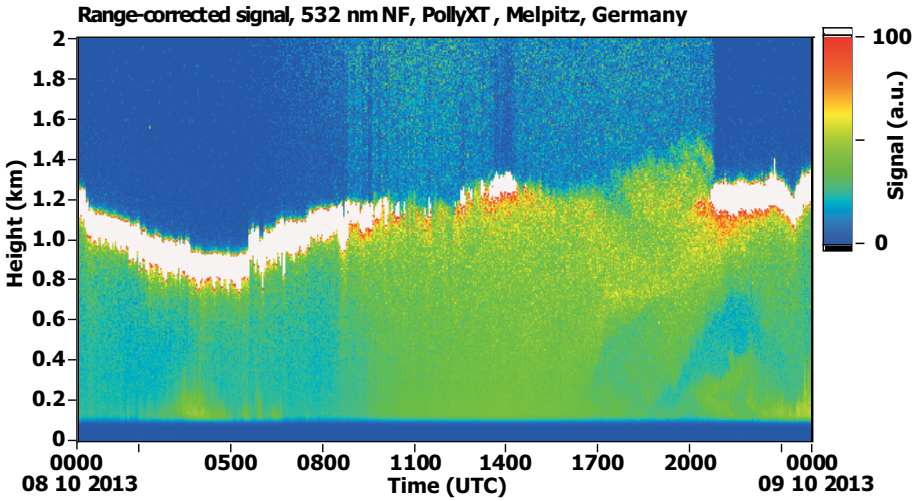

Figure 9. Lidar POLLY^{XT} measurements (532 nm backscatter signal) in Melpitz on 8 October 2013.

AMTD
7, 12283–12322, 2014

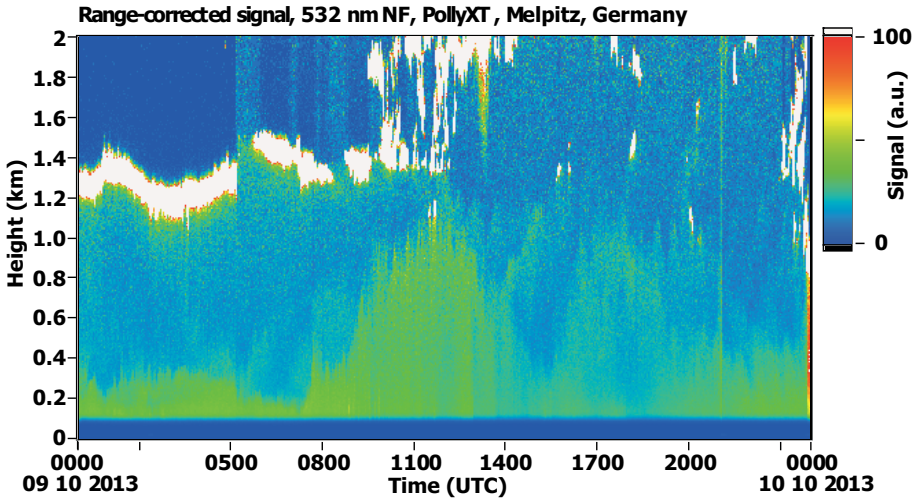

Figure 10. Lidar POLLY^{XT} measurements (532 nm backscatter signal) in Melpitz on 9 October 2013.

AMTD
7, 12283–12322, 2014

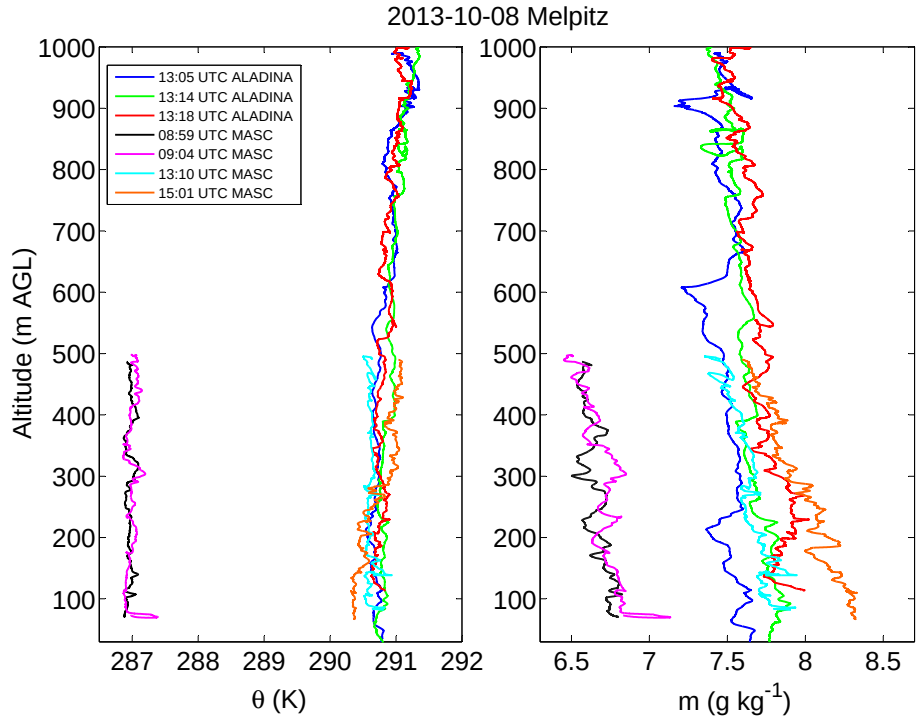

Figure 11. Vertical profiles of potential temperature Θ and mixing ratio m measured with MASC and ALADINA in Melpitz on 8 October 2013.

AMTD
7, 12283–12322, 2014

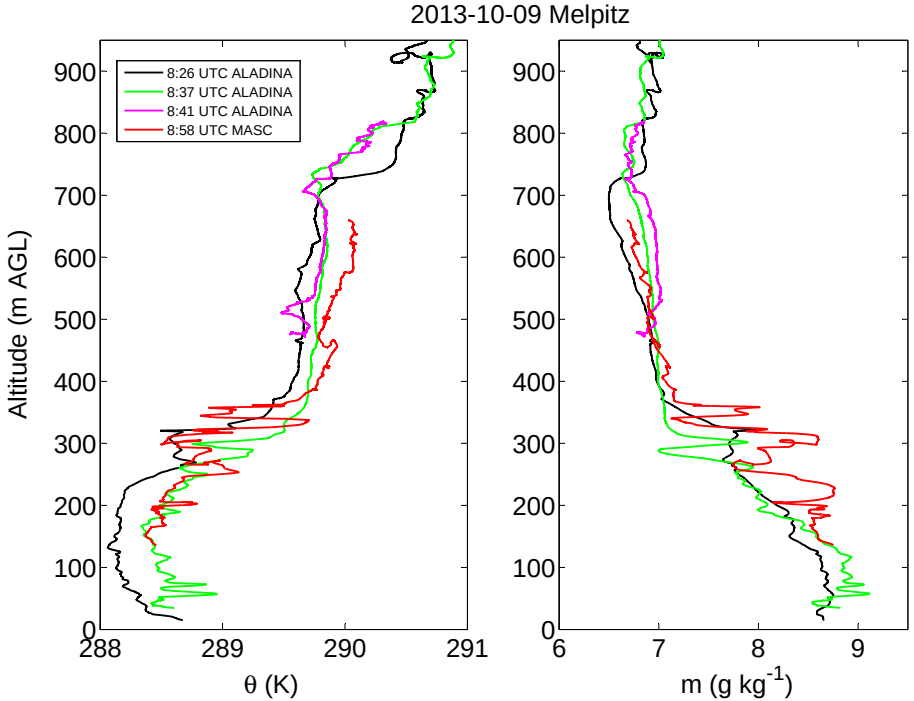

Figure 12. Vertical profiles of potential temperature Θ and mixing ratio m measured with MASC and ALADINA in Melpitz on 9 October 2013.

AMTD
7, 12283–12322, 2014

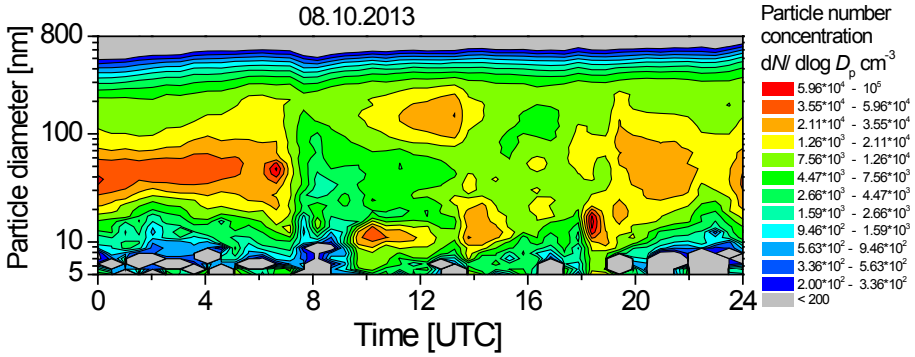

Figure 13. Aerosol number concentration measured with a TSMPS in Melpitz on 8 October 2013.

AMTD
7, 12283–12322, 2014

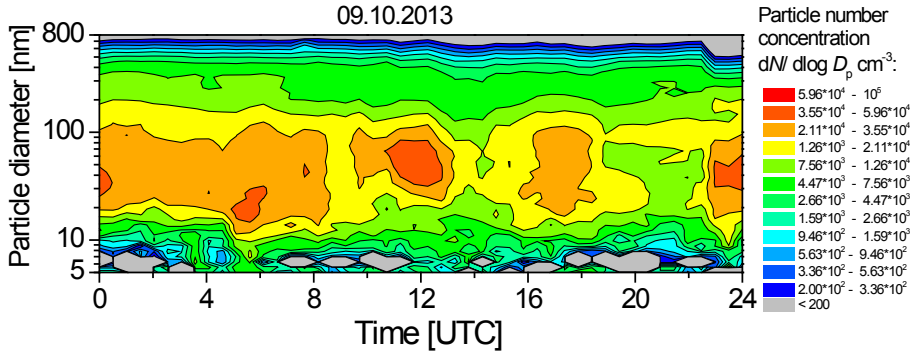

Figure 14. Aerosol number concentration measured with a TSMPS in Melpitz on 9 October 2013.

AMTD
7, 12283–12322, 2014

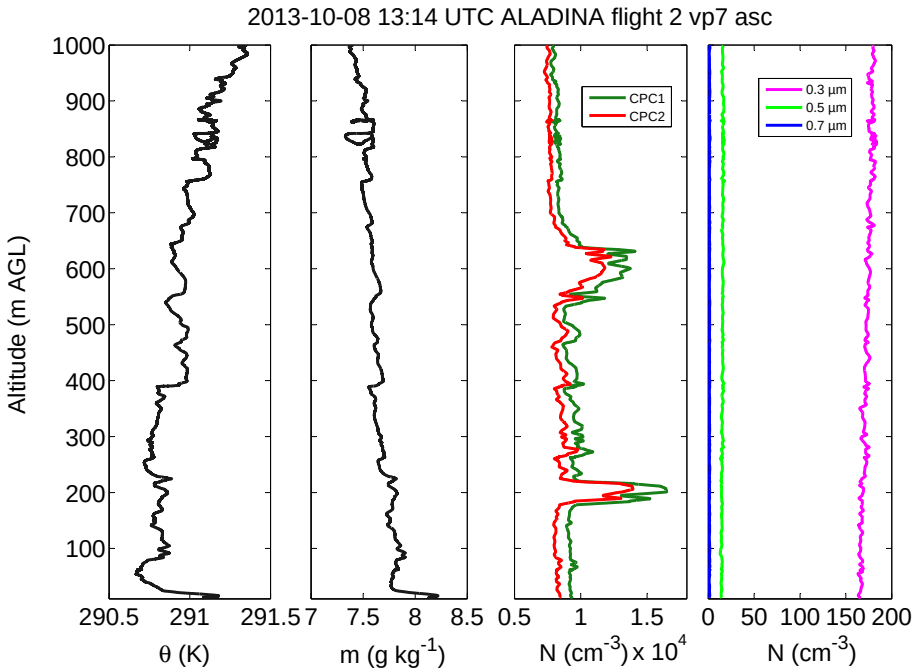

Figure 15. Vertical profiles of **(a)** potential temperature Θ, **(b)** mixing ratio m, **(c)** aerosol number concentrations for particle sizes above 11 nm (CPC1 green line) and 18 nm (CPC2, red line) and **(d)** particle number concentrations for particle sizes above 300 nm (pink line), 500 nm (bright green line) and 700 nm (blue line) detected with three OPC channels during flight 2 (ascent) in Melpitz on 8 October 2013 at 13:14 UTC.

AMTD
7, 12283–12322, 2014

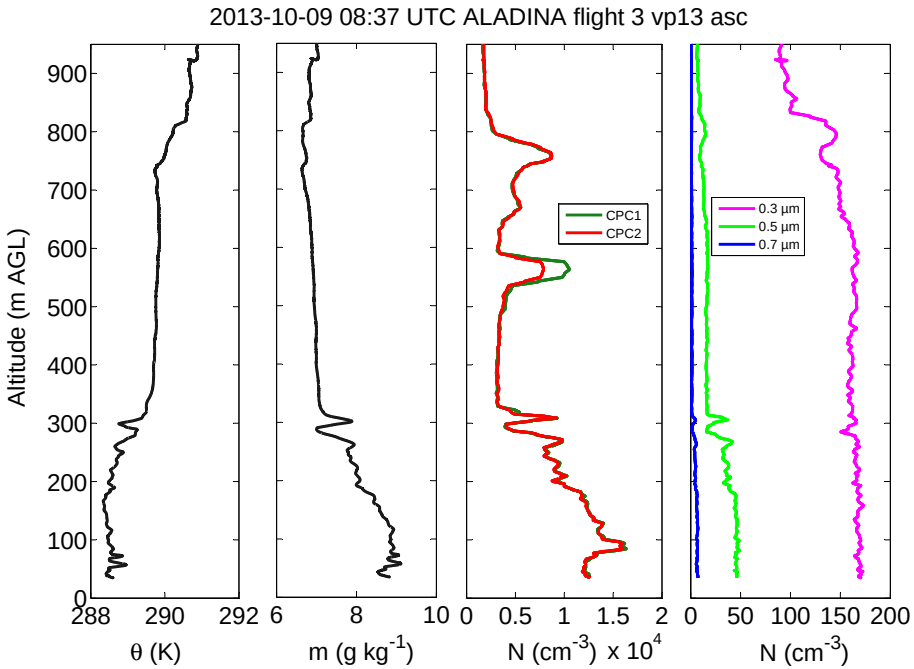

Figure 16. Same as Fig. 15 but during flight 3 (ascent) in Melpitz on 9 October 2013 at 08:37 UTC.

AMTD
7, 12283–12322, 2014